Exploiting Channel Periodicity in Body Sensor Networks

Nathan E. Roberts, Seunghyun Oh, and David D. Wentzloff, *Member, IEEE*

***Abstract*—This paper models the periodic characteristics of body sensor network (BSN) wireless channels measured using custom hardware in the 900-MHz and 2.4-GHz bands. The hardware logs received signal strength indication (RSSI) values of both bands simultaneously at a sample rate of 1.3 kS/s. Results from a measurement campaign of BSNs are shown and distilled to reveal characteristics of BSN channels that can be exploited for reducing the power of wireless communication. A new channel model is introduced to add periodicity to existing 802.15.6 WBAN path loss equations. New parameters, activity factor and location factor, are introduced to estimate the model parameters. Finally, a strategy for exploiting the periodic characteristics of the BSN channel is presented as an example, along with the power savings from using this strategy.**

***Index Terms*—Body sensor networks (BSNs), channel modeling, energy constrained systems, periodic channels, received signal strength indication (RSSI), 802.15.6 WBAN.**

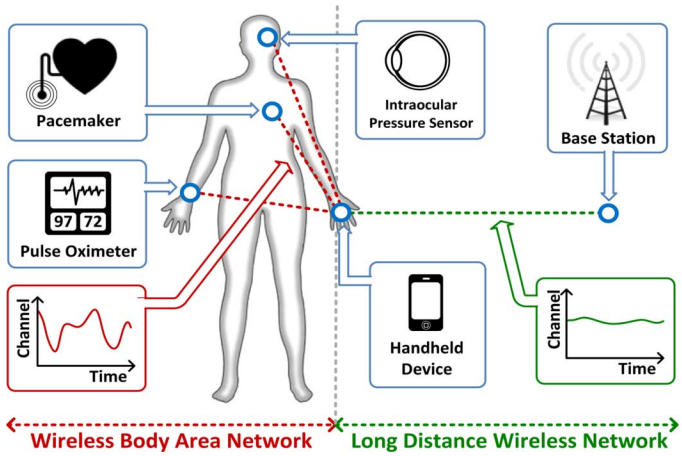

Fig. 1. Overview of wireless BSN.

I. Introduction

DEVELOPING accurate and sophisticated channel models for energy-constrained systems is a necessary step in understanding the key elements that factor into a channel model's behavior. However, channel modeling does not intuitively lend itself to aid the designer in producing system and low-level circuit design tradeoffs that are critical for improving energy efficiency. A body sensor network (BSN) is a network of miniature devices worn on the body to monitor a person's health status, for example. Fig. 1 shows an example of a BSN linking several sensing devices to a common aggregator, in this case a cellphone. By producing a model that focuses on the periodic time domain behavior of the channel for a wireless body sensor network, we can better analyze power/sensitivity tradeoffs at the circuit level and how they might impact communication goals at the system level. Similarly, accurate models can be used to develop BAN-channel specific MAC protocols that more efficiently duty-cycle the radios.

A. Channel Model Around the Human Body

The channel for wireless body sensor networks involves the environment, and electromagnetic propagation, around the human body which is complicated due to the body's effect on antenna performance [1]. One reason the channel for a BSN is unique compared to other channel models is the channel's dynamic characteristics due to the inherently limited motion of a person's body and the proximity of the sensors to the body itself. The distance and angle of antennas mounted to sensors worn on the body will constantly change in relation to one another as a person performs daily activities. For example, if a person has sensors on their belt and their wrist, then when their arm is in front of the body while walking, the channel will be line-of-sight (LOS) and the signal will be strong. In the back of their stride the channel will be nonline-of-sight (NLOS) and the signal will be weak, requiring more power to receive it. Intuitively, the channel should oscillate between strong and weak conditions as the person walks, runs, or performs other daily activities. Furthermore, these oscillations should be bounded by the physical limitations of the body's movement, or lack of movement (i.e., the human body is never perfectly still). Statistically analyzing such behavior using empirical data will allow us to effectively utilize the dynamics of the channel to reduce power consumption of the radio.

B. Low Power Radios

Radio power typically consumes the majority of the total power in a BSN and is therefore a significant bottleneck in energy efficient design. This is because radio power is typically much higher than other components in a BSN node, and the radio is not as easily duty cycled since it has to remain on when actively listening for packets. Often, as is the case with standards like Bluetooth or Zigbee, radios are designed to have excellent sensitivity, defined as the minimum detectable

Manuscript received October 20, 2011; revised January 02, 2012; accepted January 23, 2012. Date of publication March 08, 2012; date of current version April 11, 2012. This paper is based upon work supported by the National Science Foundation under Grant CNS-1035303. This paper was recommended by Guest Editor B. Otis.

The authors are with the Department of Electrical Engineering and Computer Science, University of Michigan, Ann Arbor, MI 48109 USA (e-mail: nerobert@umich.edu; austeban@umich.edu; wentzlof@umich.edu).

Color versions of one or more of the figures in this paper are available online at http://ieeexplore.ieee.org.

Digital Object Identifier 10.1109/JETCAS.2012.2187701

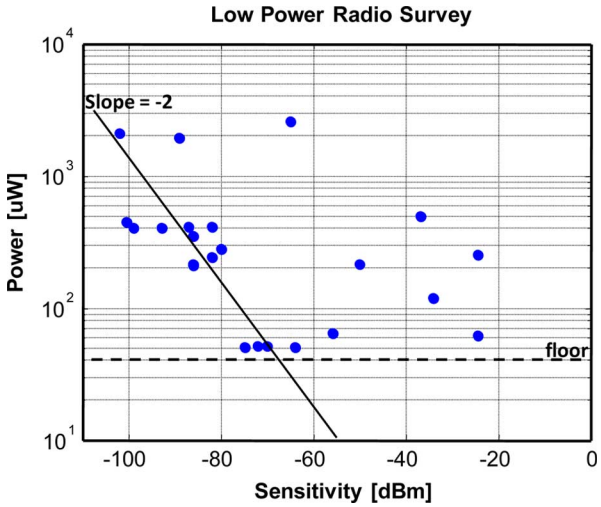

Fig. 2. Low Power Radio Survey (2006–2010) [2]–[16].

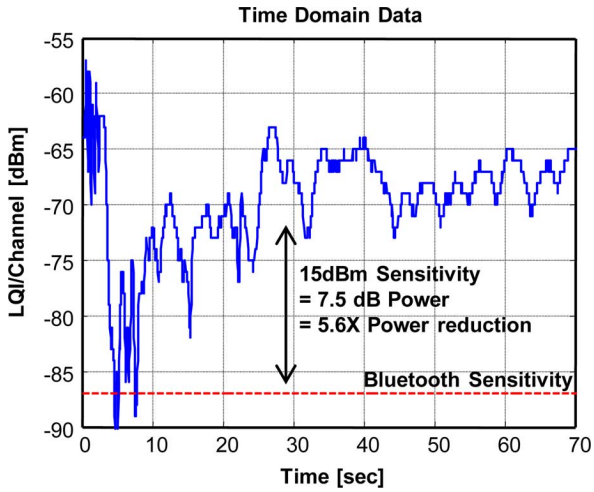

Fig. 3. Channel path loss versus Bluetooth sensitivity.

power level of the receiver, so they can operate at a near worst-case path loss. This sensitivity level ensures reliable communication, but significantly increases the radio's power budget. Fig. 2 shows a survey of published ultra-low power radios from 2006–2010, comparing their power versus sensitivity. Empirically, the survey shows a slope of -2 on a log graph between sensitivity and power consumption, with a floor around $-40\,\mu$W. The slope is influenced by several parameters, such as the variation in data rate, architecture, and nonlinearity present in the radios. The survey only covers ultra-low power receivers, common in BSN research, and Bluetooth or Zigbee receivers with higher power will sit well above this line. Using this survey one can estimate a squared relationship between power and sensitivity. For example, a $2\times$ increase in power results in a $4\times$ increase (improvement) in sensitivity.

C. Design Tradeoffs

Knowing the time domain response of a wireless BSN channel allows us to make decisions based on design tradeoffs if we can tolerate periods of interrupted communication. By reducing the sensitivity of the receiver, square root power gains can be achieved at the cost of intermittent communication. Even so, the channel variability is slow enough that efficient packet transfer is possible.

To illustrate this tradeoff, Fig. 3 shows the measured link quality indicator (LQI) versus time of a person running with a receiver on the left hip and transmitter on the left wrist. Also shown is the sensitivity of a TI Bluetooth low energy radio [17] as an example. When LQI is above the sensitivity limit, reliable communication is achieved, and in this example, the majority of the time LQI far exceeds the sensitivity; therefore, the radio is overdesigned for the given channel. One could decrease the receiver sensitivity by 15 dB in this case, which would give an estimated $5.6\times$ power reduction by applying the empirical slope from Fig. 2, but result in intermittent communication. Provided a BSN sensor can tolerate some latency, we can make use of the fact that poor quality channels do not remain poor for long when a person is active.

The key to our modeling is a focus on exploiting the periodicity of the channel and creating a model with the radio designer in mind. Section II will introduce current channel modeling progress in a wireless BSN and summarize the work done in the 802.15.6 Wireless Body Area Network (WBAN) Task Group. We will address some of the short comings of these models and explain how we plan to resolve them. Section III will introduce our custom portable dual-band RSSI recorder that can collect data in the 900-MHz and 2.4-GHz bands simultaneously. Section IV will show our measurement results and Section V will discuss our new channel model. Section VI will give examples on how this new model can influence radio design decisions. Section VII will conclude the paper.

II. Channel Modeling Background

A. Background Modeling and Equations

The 802.15.6 (WBAN) channel model document [18] is a collection of multiple experiments spanning different defined channels, including body-to-body or body-to-off body communication as well as line-of-sight (LOS) and nonline-of-sight (NLOS) variations. The purpose of these channel models is for evaluating potential physical layer proposals more than producing all-encompassing models. The ones included below describe WBAN CM3, which is body-to-body communication in the 900-MHz and 2.4-GHz bands for both LOS and NLOS communication. Three different experiments are described, resulting in the following two path loss modeling equations:

$$\mathrm{PL}(d)\ [\mathrm{dB}] = a\log_{10}(d) + b + N \tag{1}$$

where a and b are coefficients of linear fitting, d is the Tx-Rx distance in millimeters, and N is a normally distributed random variable with σ_{n}

$$\mathrm{PL}(d)\ [\mathrm{dB}] = -10\log_{10}\left(P_0 e^{-m_0 d} + P_1\right) + \sigma_p n_p \tag{2}$$

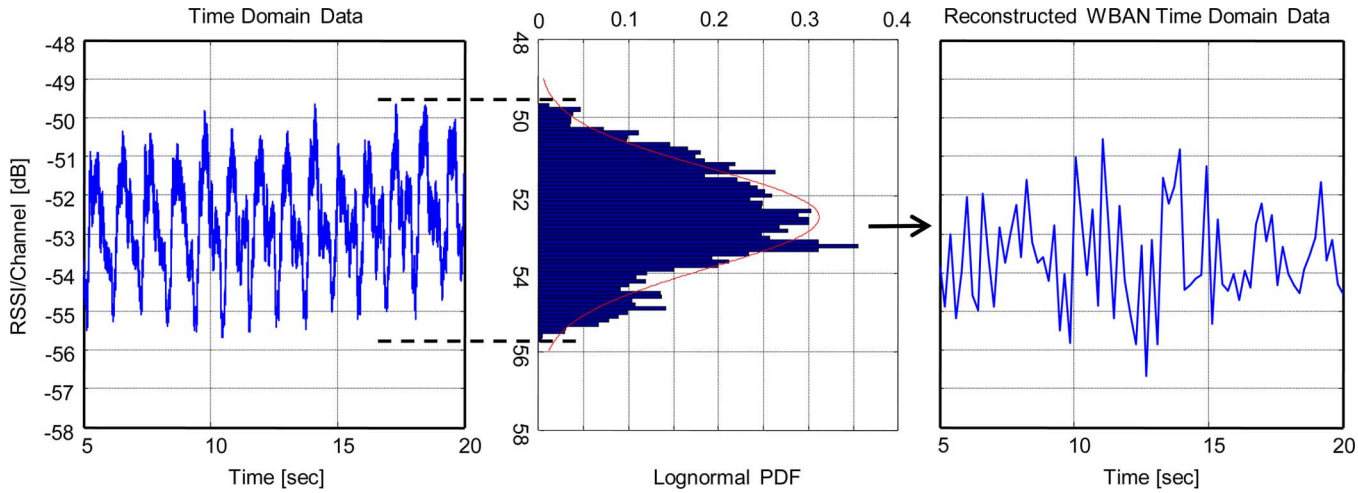

Fig. 4. Time domain channel model with WBAN (1) reconstruction.

where P_0 is the average loss close to antenna, m_0 is the average decay rate in dB/cm for the surface wave traveling around the perimeter of the body, P_1 is the average attenuation of components in an indoor environment radiated away from the body and reflected back toward the receiving antenna, $\sigma_{\rm p}$ is the lognormal variance in dB, and n_p is a zero mean unit variance Gaussian random variable.

Equation 1 references Experiment A in the Channel Modeling document [19] which features a test subject in a hospital room in different stationary positions. S21 is measured between two antennas using a vector network analyzer in the 950–956 MHz and 2.4–2.5 GHz bands. A transmitter antenna is placed at the waist, with a receiver antenna being placed on parts of the body, including head, ear, shoulder, wrist, waist, leg, and ankle. Measurements in an anechoic chamber are also taken as a control experiment to remove the multipath effect. The path loss model is derived using a regression line through least square fitting for each frequency band.

Equation 2 references Experiment B [20] which is similar but includes signal fading in its experiments, covering the 915-MHz and 2.45-GHz frequency band. Antennas are placed horizontally around the torso as well as vertically along it and S21 is measured similar to Experiment A. The test subject is standing still during the experiments.

Experiment C [21] observes subject movement. Test subjects are observed standing, walking, and running in place in an office environment using BPSK modulated signals at 820 and 2360 MHz. The channel response is captured on a vector signal analyzer in 40 μs sets, with a 2.5-ms gap before the next capture (sample rate of 0.4 kS/s), totaling 10 s. Results show the most significant fading effects are due to movement and the change in distance and alignment of the antennas. Variation also increases with increased movement from the test subject. Finally, channel stability over time is observed and assigned a value, the channel variation factor, which is the ratio between the standard deviation and the rms power of the sequence.

Papers published outside of 802.15.6 cover a spectrum of different approaches ranging from parallel finite-difference time-domain method (FDTD) simulations [22] to measurements from commercial MICAz motes using a Zigbee radio [23]. Papers have also attempted to characterize the temporal characteristics of the channel [24].

B. Results From Channel Modeling Background Study

Many different distributions such as lognormal, normal, or Weibull [25] fit different experimentation scenarios within a BSN. The most commonly used distribution for a static channel is lognormal, supported by both the S21 and RSSI data collection. Different experiments show different adjustment factors to the basic lognormal equation. The lognormal result is explained in [25] by the large number of contributing effects to the attenuation of the transmitted signal which are multiplicative, or additive in the log domain. In addition, movement was shown to increase the variability of the channel, which is an important observation for BSNs. Several papers cite the significant impact of antenna angles as well as influences from the environment (multipath) and the size and shape of the user [22].

There are several factors that these experiments lack that are critical to applying our knowledge of the channel to the design of an energy efficient BSN. Most experiments do not attempt to characterize the time domain characteristics of the channel and are therefore not conducted with a high enough sample rate or for a long enough period of time to accurately see the influence time has on the channel.

Perhaps most important is that the resulting path loss equations erase time domain periodicity from the test results. Fig. 4 illustrates how this periodicity is erased when using only path loss statistics. A measured time domain channel response is shown (left) with its respective distribution (middle), which is then reconstructed using (1) from the WBAN task group channel model (right). It is obvious that (1) does not reproduce the structured periodic channel response in the original measured data, nor is that its intention. The purpose of (1) is to give a single path loss estimate for a channel. The time domain information is lost.

Understanding this variability and being able to anticipate or accommodate for it is the key to our channel model and subsequent analysis. Our channel modeling will correct these short-

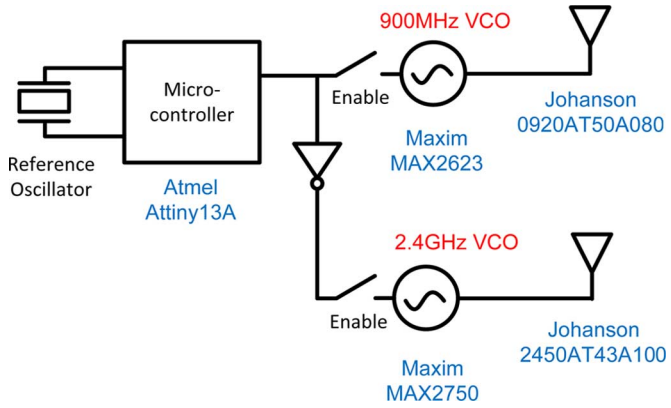

Fig. 5. Schematic of the transmitter.

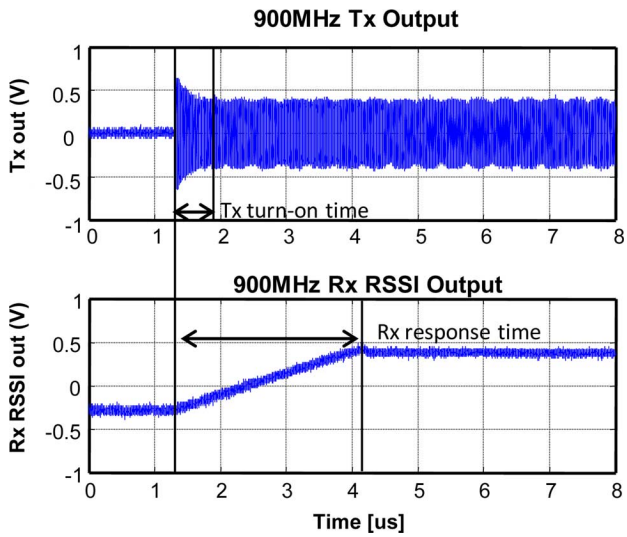

Fig. 6. Transient response.

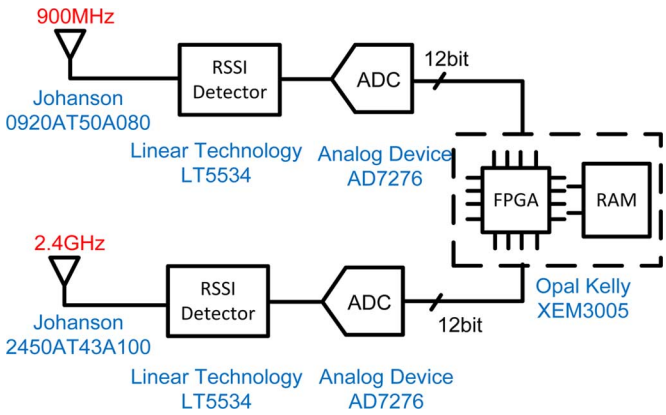

Fig. 7. Schematic of the receiver.

comings by using our custom COTS hardware to measure RSSI at a 1.3 kS/s sample rate. Since the hardware is battery operated and portable, we can take data in different environments very applicable to peoples' normal lives or specific medical applications. Our statistical models will evaluate path loss of the channel in the time domain and will develop a policy to characterize the channel so it can be simplified and used to make design decisions that impact the performance and energy consumption of a BSN node.

III. Portable Dual-Band RSSI Recorder

RSSI was measured in the 900-MHz and 2.4-GHz bands to model channel characteristics. Multiple transmitters are placed on the body and broadcast simultaneous 900-MHz and 2.4-GHz tones. These tones are on–off-keying (OOK) modulated with unique CDMA codes so that the receiver can identify each transmitter. Multiple receivers are placed on the body and simultaneously record the RSSI of the 900-MHz and 2.4-GHz paths into local memory. When an experiment is complete, the RSSI data is uploaded to a PC, where postprocessing is performed to correlate the data with the CDMA code, which will identify the transmitter and provide accurate RSSI measurements.

The primary advantages of our hardware are that it is dual-band, portable, and has a sampling rate sufficient for Nyquist sampling of the channel response. The transmitter and receiver each have two antennas at 900 MHz and 2.4 GHz. Additionally, they can operate with a single portable battery. The sampling rate of the channel RSSI can be programmed up to 50 kS/s. In this work, a sampling rate of 1.34 kS/s was chosen to increase sampling duration.

A. Transmitter

Fig. 5 shows the schematic of the transmitter. It consists of a crystal oscillator, a microcontroller, a 900-MHz oscillator (MAX2623 from MAXIM), a 2.4-GHz oscillator (MAX2750 from MAXIM), a 900-MHz antenna (0920AT50A080 from Johanson Technology) and a 2.4-GHz antenna (2450AT43A100 from Johanson Technology). A 5-MHz crystal oscillator is used as a reference clock, and a single 3 V coin-sized battery is used to supply power to the entire transmitter.

The microcontroller generates a unique CDMA code for each transmitter and performs OOK by enabling the 900-MHz and 2.4-GHz VCOs with it. The enable signals for the VCOs are inverted to eliminate interference between the bands.

The one-bit time duration of the CDMA code is 24 μs. As shown in Fig. 6, this duration is much longer than the 1 μs turn-on time of the VCO and the 3 μs response time of the RSSI IC in the receiver. The supply current of the entire transmitter is 12.8 mA, which can be powered continuously from a single 3 V battery for 48 h.

B. Receiver

Fig. 7 shows the schematic of the receiver. It consists of a 900-MHz antenna (0920AT50A080 from Johanson Technology), a 2.4-GHz antenna (2450AT43A100 from Johanson Technology), two RSSI detectors (LT 5534 from Linear Technology), two ADCs (AD7276 from Analog Devices), an FPGA (Xilinx Spartan-3E), and 32 MB of SDRAM.

Each 900-MHz and 2.4-GHz signal is received through the antennas, and then RSSI detectors convert the received signal strengths to analog voltage outputs. The 12-bit ADCs convert these analog voltages to digital values at a programmable sampling rate. A 167 kS/s sampling rate is chosen to ensure four sample points are recorded per CDMA bit. For a 31-bit CDMA code, this results in a sample rate of $167/31/4 = 1.3$ kS/s

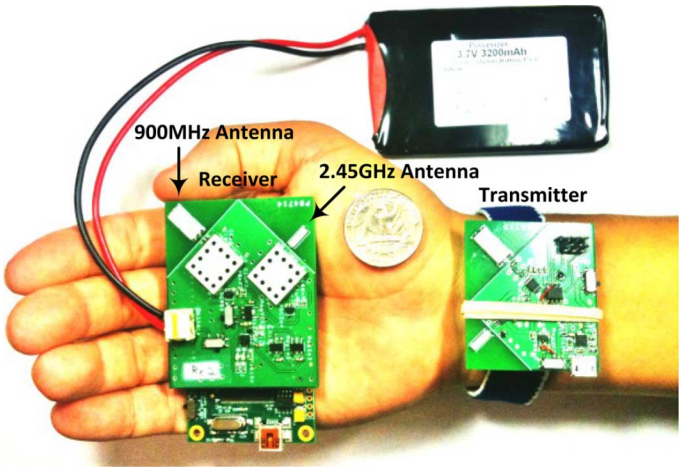

Fig. 8. Photograph of the transmitter and receiver.

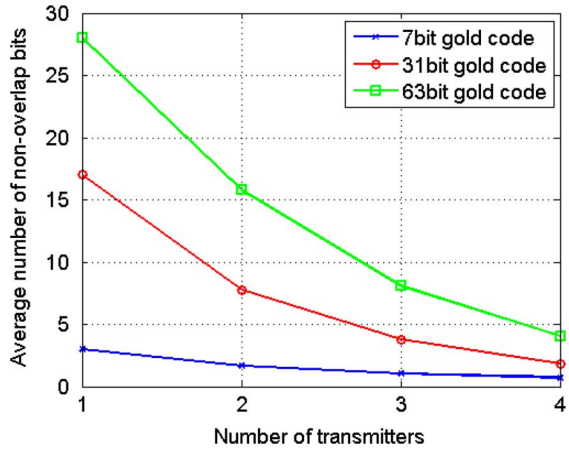

Fig. 9. Number of transmitters versus nonoverlapping bits.

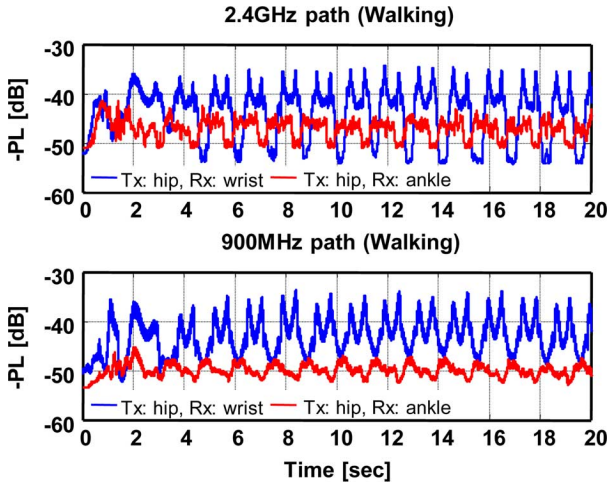

Fig. 10. Data showing correlating band and location measurements.

after averaging. The supply current of the whole receiver is 184 mA, which can continuously operate with a rechargeable battery for 17.4 h. The receiver also has a power management chip, BQ24072 from Texas Instruments, so that it can charge the battery when it is connected to a USB cable.

Fig. 8 shows a photoggraph of the transmitter and receiver. The size of the transmitter and receiver PCBs are 45 mm $\times$ 40 mm and 48 mm $\times$ 60 mm, respectively. A wrist strap is tied to the transmitter to make it easy to wear.

C. Support for Multiple Transmitters

To measure the correlation of multiple nodes on the body, each transmitter sends its unique Gold code. Gold codes are a set of binary sequences, where the cross-correlation of each sequence is bounded into three values. Gold codes are commonly used when implementing CDMA as they allow the receiver to easily identify the corresponding transmitter which sent the signal of interest [26].

Since RSSI values are not linear but logarithmic, an interval is required in which the received power from only one transmitter is observed by the receiver in a given band in order to extract the RSSI value from that transmitter alone. As the length of the Gold code increases, the probability of having a nonoverlapping bit also increases; however, the symbol duration will increase such that the channel sampling rate decreases. Therefore, a trade-off exists between the length of the Gold code and the number of transmitters supported. Fig. 9 shows the number of transmitters versus the average number of nonoverlapping bits of each Gold code, considering random shifts between all received Gold codes. In this work, the system is designed for a maximum of four transmitters; therefore, a 31-bit code is chosen.

IV. Channel Measurements

The purpose of the measurement campaign was to collect data across enough controlled scenarios that we could generalize the results and compute various modeling factors. In addition we collected data correlation between bands and sensor locations. We did this in two stages: controlled experiments followed by measurements conducted in a real-life scenario. Each measurement was repeated three times for redundancy. Different locations on the body were targeted for each experiment.

A. Controlled Experiments

Fig. 10 shows the hardware's ability to simultaneously measure 900 MHz and 2.4 GHz bands at multiple locations at the same time. In this figure, path loss is shown between hip-to-wrist and hip-to-ankle in both RF bands, sampled at 1.3 kS/s, for a period of 20 s. To calculate the path loss, including antenna gain, we subtracted the transmit power (-3 dBm) from the RSSI measurement. Fig. 11 highlights variations in the channel periodicity for differing activity levels as well as the hardware's noise floor which is around a path loss of -54 dB.

For different scenarios, the data that shows the most variability in the channel, as expected, comes from sensors on the body extremities that move the most, like the ankle or wrist. Somewhat unexpected is sensors on the body's core like the hip or chest also show a periodic response. Even with a person standing still, faint periodicity can be observed.

B. Observations

Some notable observations from controlled experiments are outlined in the following paragraphs.

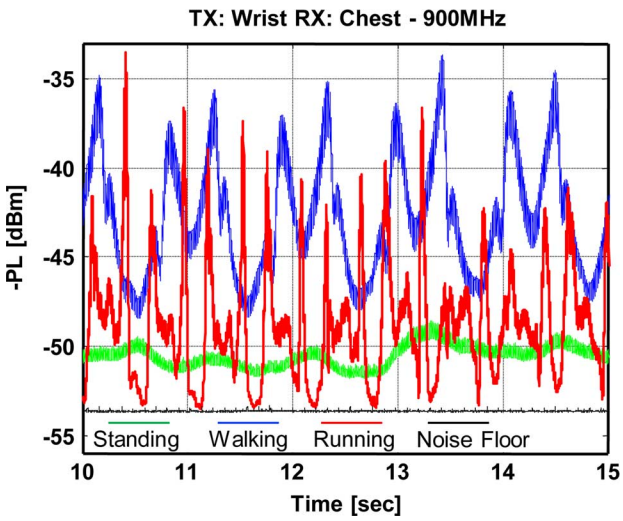

Fig. 11. Data showing activity variations.

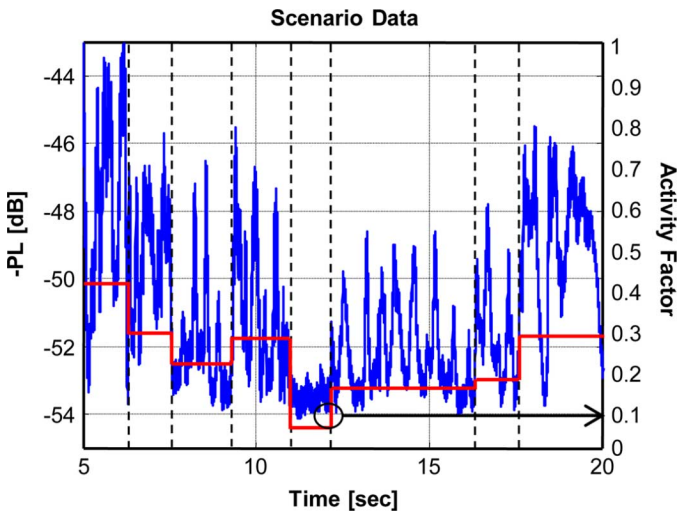

Fig. 12. Channel waveform of a real-life scenario.

Hip-to-chest and hip-to-wrist communication produces periodic signals with more frequency content than chest-to-chest or chest-to-write, which is due to the motion of the hip sensor. Hip to chest communication appears as a noisy sinusoid. When a person walks the hip will swing between LOS and NLOS with the chest sensor, which creates the sinusoidal response and the frequency content appears due to the forward and backward motion between the hip and chest as the person lifts and lowers their leg. The movement of the hip and the swing of the wrist both contribute to the extra frequency content in that scenario.

The channel between the hip and ankle looks similar to a square wave when walking and the increased frequency when running makes it appear more sinusoidal. The channel between both wrists is poor due to the nearly constant NLOS condition, therefore relying mostly on multipath for communication. When running, if the user is leaning forward, small windows where the wrists pass by each other, yet are still in front of the body and therefore LOS, will produce pulse shapes in the path loss. Channel Measurement statistics are summarized in Table I. The superscript numbers represent which sets of data were taken simultaneously. The frequency column is the fundamental frequency of the oscillations observed in the path loss. μ and σ are the mean and standard deviation of the path loss calculated in dB. The two numbers in each cell represent 900-MHz and 2.4-GHz data, respectively.

TABLE I
MEASURED CHANNEL PL PARAMETERS (TWO NUMBERS REPRESENT 900 MHZ/2.4 GHZ DATA) (SUPERSCRIPT SHOWS SIMULTANEOUS DATA COLLECTION)

900/2400MHz	TX/RX	Freq [Hz]	μ [dBm]	σ [dB]
Standing	Hip/Ankle[1]	0.13/0.13	49.60/44.30	0.28/0.30
	Hip/Wrist[1]	0.28/0.17	50.34/48.74	0.90/0.99
	Wrist/Wrist[2]	0.15/0.15	53.40/53.66	0.08/0.08
	Wrist/Chest[2]	0.13/0.13	52.94/50.00	0.16/0.34
	Chest/Hip[3]	0.13/0.17	47.64/47.46	0.56/0.62
	Chest/Wrist[3]	0.15/0.15	52.75/50.70	0.20/0.93
Walking	Hip/Ankle[1]	0.99/0.99	50.24/47.55	1.13/1.85
	Hip/Wrist[1]	0.96/0.96	43.92/43.78	3.22/5.25
	Wrist/Wrist[2]	0.13/0.13	53.54/54.00	0.24/0.39
	Wrist/Chest[2]	0.97/0.97	52.13/49.68	1.51/0.80
	Chest/Hip[3]	0.68/0.92	47.24/45.92	1.20/1.43
	Chest/Wrist[3]	0.93/0.93	50.84/49.79	2.54/3.96
Running	Hip/Ankle[1]	1.78/1.78	50.70/49.77	1.48/1.24
	Hip/Wrist[1]	1.80/1.70	49.57/47.81	2.92/4.32
	Wrist/Wrist[2]	1.60/1.80	53.47/53.61	0.25/0.81
	Wrist/Chest[2]	1.76/1.74	51.37/46.45	2.28/4.33
	Chest/Hip[3]	1.71/1.72	46.93/47.16	1.62/1.93
	Chest/Wrist[3]	1.72/1.72	46.19/43.4	3.90/6.93

C. Scenario Experiment

The second set of measurements in Fig. 12 targeted a real life scenario where the user does not conduct strictly repetitive motions, therefore creating a nonuniform channel. The scenario involved the test subject playing tennis outdoors which involves lots of fast, abrupt movements in an outdoor environment with the receiver on the left hip and transmitter on the left wrist. Since the channel is nonuniform, nonuniform windowing was also used to break the channel data into smaller segments that were analyzed for periodicity. The time domain channel response and resulting activity factors (defined in Section V) plotted across time are shown in Fig. 12. The purpose of this experiment was to observe natural movement and the change in frequency and standard deviation across time. It is possible that a person will remain stationary for a given period of time in a way that restricts communication between sensors. However, the data shows that a person in motion will see periodic peaks and valleys in the channel response between sensors, therefore allowing communication in at least some periods of time.

D. Correlation Among Sensor Locations and Bands

In addition to collecting data for the development of a model, we correlated the channel response of different sensor locations

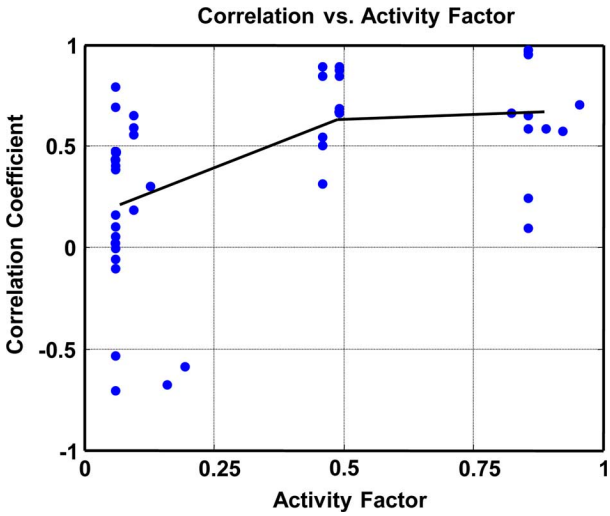

Fig. 13. Correlation between bands.

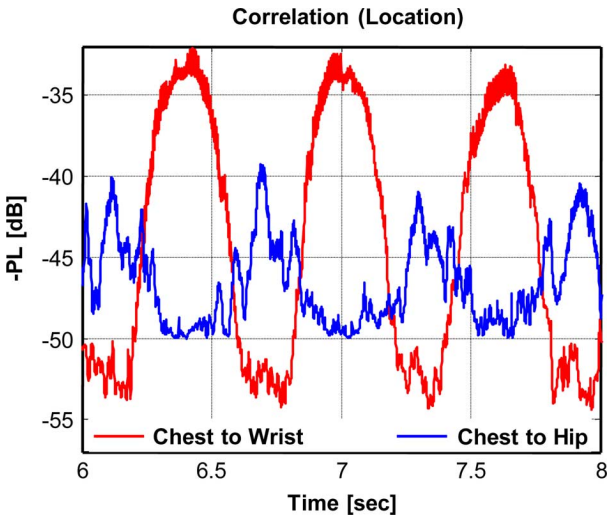

Fig. 14. Correlation between locations.

on the body as well as different frequency bands. This information is useful in BSN applications that may want to use knowledge of one channel to predict the quality of another channel to a different location on the body or in a different band for asymmetric wireless links [27].

Frequency correlation is calculated by taking the correlation coefficient between the 900-MHz and 2.4-GHz bands of the same experiment. Results can be seen in Fig. 13. Frequency correlation increases in relation to motion. The correlation coefficient while standing is difficult to predict, with values being essentially random, ranging from 0.78 to -0.72. Once the test subject starts moving, correlations increase significantly with gradual improvement between walking and running. One conclusion we can draw from this is that while a person is stationary, and a good channel is observed in one frequency band, it is no guarantee that another frequency band will be good. However, when the person is active, there is high probability that both bands will have good channels at the same time.

The correlation among sensor locations that was the strongest involved sensors from the wrist and hip communicating with a

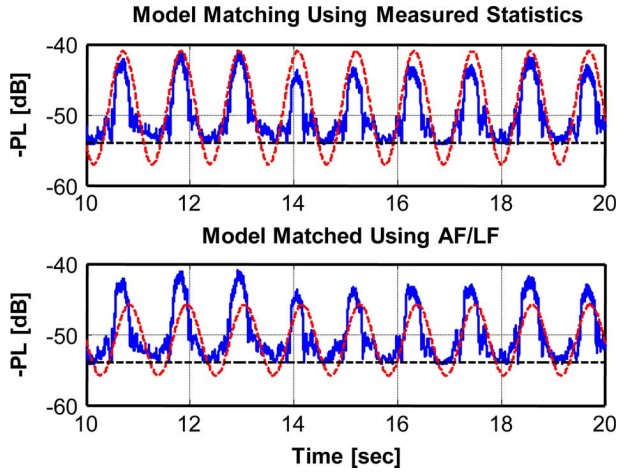

Fig. 15. Model validation.

sensor on the chest. This scenario, shown in Fig. 14, had a negative correlation coefficient of -0.73 and is a result of one sensor being placed on the upper half of the body (wrist) and lower half (hip). While the test subject was moving, the wrist would swing forward and into a LOS scenario with the sensor on the chest while the hip would be moving backwards and out of LOS communication. This type of location correlation can be exploited for multihop routing, or if sensors are on the same side of the body and placed on opposing extremities so that one sensor is always in good communication while walking or running. The communication location that had the least correlation was wrist to wrist.

V. Periodic BSN Channel Model

Our goal is to gain insight into the channel and develop simplified models that aid in the system level design of radios for BSNs. This includes observing path loss in different scenarios as well as developing correlations between multiple sensors at different locations on the body and between different frequency bands. The controlled experiments, shown in Table I, are aimed to characterize the complex BSN channel as simply as possible to allow for quick and effective design calculations.

The periodic behavior of the channel seen in the data is relatively sinusoidal and can be represented as such. The proposed path loss of the periodic BSN channel model with respect to time is

$$\mathrm{PL}(t)[\mathrm{dB}] = \mathrm{PL}(d) + 2\sigma_{PL}\sin(2\pi \cdot f_{\mathrm{PL}} \cdot t) \qquad (3)$$

where $\mathrm{PL}(d)$ is the path loss in dB calculated from one of the 802.15.6 [18] models [e.g., (1) or (2)], and the second term adds the modeled channel periodicity where σ_{PL} is the standard deviation, in dB, and f_{PL} is the fundamental path loss repetition frequency.

This model complements the WBAN equations that calculate path loss, by adding a periodic dimension to the equation which accounts for the periodicity we measured in the channel. Using measured statistics, (3) closely models the channel as seen in the top plot of Fig. 15, which represents someone walking with

TABLE II
ACTIVITY AND LOCATION FACTORS DERIVED FROM DATA

Action	TX/RX	Activity Factor	Location Factor
STANDING	Hip/Ankle	0.07	0.24
	Hip/Wrist		0.70
WALKING	Wrist/Wrist	0.45	1.00
	Wrist/Chest		0.60
RUNNING	Chest/Hip	0.85	0.24
	Chest/Wrist		0.60

a transmitter on their wrist and receiver on their chest. Note the model drops below the hardware's noise floor.

A. Impact of Activity and Location

Numerous individual factors contribute to the path loss and periodicity of the channel including antenna placement and direction, multipath, and body shape. To integrate all these factors would produce a complicated model that would not be practical for BSN design. To generalize the results of our channel modeling measurement campaign we will introduce two variables that will account for all the different factors in a simple and intuitive way. Even though extremely simple by design, these factors are shown to predict the channel response with accuracy sufficient for BSN design. The two variables are activity factor (AF) and location factor (LF)

$$\text{Activity Factor (AF)} = \text{amount of user movement.} \quad (4)$$

AF is a qualitative number between 0 and 1 that is approximated by knowing what a person is doing. If a person is completely still the AF is 0 and a full sprint is 1. Activity between these extremes is qualitatively assigned an intermediate number based on a best guess as to the relative level of activity. For example, $\text{AF} = 0.25$ is someone working at a computer, $\text{AF} = 0.5$ is someone walking, and $\text{AF} = 0.75$ is someone jogging. The frequency component of the path loss in (3) is then calculated as

$$f_{\text{PL}} = f_{\max} \cdot \text{AF} \quad (5)$$

where $f_{\max}$ is the maximum capable frequency of the user's movement, which we assume is 2 Hz which is a good general assumption. Under normal circumstances, it is highly unlikely that an average person would exceed a fundamental repetition rate greater than 2 Hz. From (5) we back-calculate the activity factor for our measured results, which are reported in Table II.

σ_{PL} in (3) is dependent on AF, as well as a LF. LF is a qualitative measure of the relative motion between two sensors, normalized between 0 and 1. An LF of 1 represents sensor locations that have a lot of movement relative to each other, e.g., wrist-to-wrist communication. An LF of 0 represents sensor locations with little to no relative movement, e.g., two sensors on the chest. Location factor between these extremes is qualitatively assigned an intermediate number, e.g., $\text{LF} = 0.25$ for hip-to-ankle, $\text{LF} = 0.5$ for chest-to-wrist, and $\text{LF} = 0.75$ is hip-to-wrist. σ_{PL} used in (3) is then calculated as

$$\sigma_{\text{PL}} = k_\sigma \cdot \text{LF} \cdot \log_{10}(1 + f_{\text{PL}}) \quad (6)$$

where k_σ is a data fitting parameter. Based on our controlled experiments, ranging from standing to running with sensors at various locations, $k_\sigma = 15$ results in the best overall fit.

The bottom plot of Fig. 15 shows the periodic model compared to the same walking data as the top of the plot, but this time using AF and LF. Using an AF and LF of 0.45 and 0.6, respectively, show a close match, which is also close to our estimates of an AF of 0.5 for walking and an LF of 0.5 for chest to wrist communication.

VI. IMPACT ON RADIO DESIGN

If we assumed that the transmitted power and antenna gain are 0 dBm and 0 dB, respectively, then we can claim that the sensitivity of the receiver is equivalent to the measured path loss. Using our developed channel model we can determine the tradeoff between communication time and receiver power using representative receivers from literature: a low power receiver [15] and a wake up receiver [7]. We will also include a commercial Bluetooth low energy radio [17] for comparison.

A. Power Savings

Using the same channel data plotted in Fig. 15 with computed AF, LF, and PL(d) values of 0.45, 0.6, and -52 dB, respectively, we can compare the performance of the two low power radios. A radio [15] with a power of 2.1 mW and a sensitivity of -100 dBm would be the primary receiver in the BSN and always remain active. At 100% operation the total power would be 2.1 mW and it can communicate 100% of the time. Using the wakeup receiver [7] with a sensitivity of -56 dBm, one can turn off the main receiver to save energy while leaving the wake up receiver always listening for packets, or even utilize the wake up receiver for low speed communication. By applying variables determined from our channel model we calculate the percentage of time the wake up receiver can communicate as

$$T_p = \frac{\pi/2 - \arcsin((S_{\text{RX}} - PL(d))/2\sigma_{\text{PL}})}{\pi} \quad (7)$$

where S_{RX} is the sensitivity of the receiver and σ_{PL} is calculated from (6) and (7), respectively. Using (8), we determine the wake up receiver will communicate 64% of the time at a power consumption of 65 μW. Utilizing channel periodicity by reducing the receiver sensitivity results in a $32\times$ power savings over the standard low power radio while being able to communicate in 64% of the channel compared to 100%. Comparing against the commercial Bluetooth radio, with a power of 58.6 mW and a sensitivity of -87 dBm, this results in a $900\times$ power savings.

B. Communication Performance

Assuming a MAC that reacts to the periodicity of the channel and knowing the percentage of time one can communicate, the time interval spent in the good channel region can be calculated. Continuing with our example; given 64% communication time and a frequency of 0.9 Hz, we can estimate the channel to be

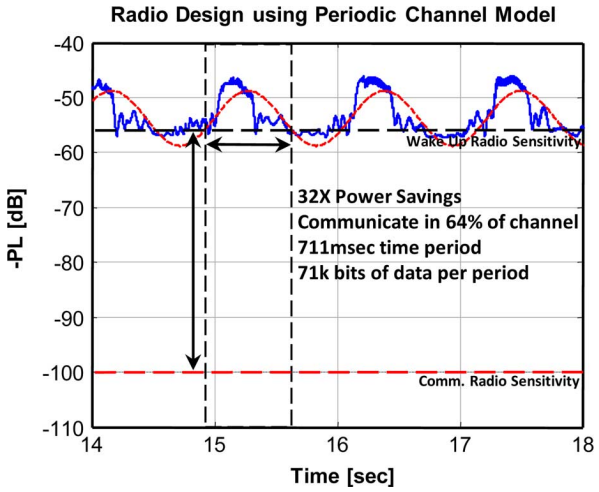

Fig. 16. Radio design.

good for 711 ms at a time. Knowing the wake up receiver has a data rate of 100 kb/s; one can transmit roughly 71 kb of information during these periods of good channel communication as seen in Fig. 16.

VII. Conclusion

In this paper, we proposed a simplified channel model to complement the current WBAN path loss models by exploiting channel periodicity in a BSN. We introduced custom hardware used to collect the data needed for this analysis and the measurement campaign designed to develop the model. We introduced Activity and Location factors to allow computation of the model's parameters. We demonstrated this model by fitting it to data collected during the measurement campaign. Finally, by making informed decisions regarding these tradeoffs we were able to show a power efficient design improvement example.

Acknowledgment

The authors would like to thank J. K. Oh for his assistance in the data collection and A. Wysocki for his assistance in the hardware prototyping.

References

[1] P. S. Hall *et al.*, "Antennas and propagation for on-body communication systems," *IEEE Antennas Propagat. Mag.*, vol. 49, no. 3, pp. 41–58, Jun. 2007.

[2] S. Drago *et al.*, "A 2.4 GHz 830 pJ/bit duty-cycled wake-up receiver with -82 dBm sensitivity for crystal-less wireless sensor nodes," in *IEEE Int. Solid-State Circuit Conf. Dig. Tech. Papers*, Feb. 2010, pp. 224–225.

[3] X. Huang *et al.*, "A 2.4 GHz/915 MHz 51 μW wake-up receiver with offset and noise suppression," in *IEEE Int. Solid-State Circuit Conf. Dig. Tech. Papers*, Feb. 2010, pp. 222–223.

[4] N. M. Pletcher *et al.*, "A 2 GHz 52 μW wake-up receiver with -72 dBm sensitivity using uncertain—If architecture," in *IEEE Int. Solid-State Circuit Conf. Dig. Tech. Papers*, Feb. 2008, pp. 524–633.

[5] J. Ayers *et al.*, "An ultralow-power receiver for wireless sensor networks," *IEEE J. Solid-State Circuits*, vol. 45, no. 9, pp. 1759–1769, Sep. 2010.

[6] B. Otis *et al.*, "A 400 μW-RX, 1.6 mW-TX super-regenerative transceiver for wireless sensor networks," in *IEEE Int. Solid-State Circuit Conf. Dig. Tech. Papers*, Feb. 2005, pp. 396–606.

[7] N. Pletcher *et al.*, "A 65 μW, 1.9 GHz RF to digital baseband wakeup receiver for wireless sensor nodes," in *Custom Integrated Circuits Conf.*, Sep. 2007, pp. 539–542.

[8] D. C. Daly and A. P. Chandrakasan, "An energy-efficient OOK transceiver for wireless sensor networks," *IEEE J. Solid-State Circuits*, vol. 42, no. 5, pp. 1003–1011, May 2007.

[9] J. Ayers *et al.*, "A 0.4 nJ/b 900 MHz CMOS BFSK super-regenerative receiver," in *Custom Integrated Circuits Conf.*, Sep. 2008.

[10] S. Gambini *et al.*, "A fully integrated, 300 pJ/bit, dual mode wireless transceiver for cm-range interconnects," in *IEEE Symp. VLSI Circuits*, Jun. 2010, pp. 31–32.

[11] R. van Langevelde *et al.*, "An ultra-low-power 868/915 MHz RF transceiver for wireless sensor network applications," in *Proc. IEEE Radio Frequency Int. Circuits Symp.*, June 2009, pp. 113–116.

[12] J. Ayers *et al.*, "A 2.4 GHz wireless transceiver with 0.95 nJ/b link energy for multi-hop battery-free wireless sensor networks," in *IEEE Symp. VLSI Circuits*, Jun. 2010, pp. 29–30.

[13] J. L. Bohorquez *et al.*, "A 350 μW CMOS MSK transmitter and 400 μW OOK super-regenerative receiver for medical implant communications," in *IEEE Symp. VLSI Circuits*, Jun. 2008, pp. 32–33.

[14] E. Lee *et al.*, "A 400 MHz RF transceiver for implantable biomedical micro-stimulators," in *Custom Integrated Circuits Conf.*, Sep. 2007.

[15] A. C. W. Wong *et al.*, "A 1 V wireless transceiver for an ultra-low power SoC for biotelemetry applications," in *Solid State Circuits Conf. ESSCIRC*, Sep. 2007, pp. 127–130.

[16] H. Yan *et al.*, "A 120 μW fully-integrated BPSK receiver in 90 nm CMOS," in *Proc. IEEE Radio Frequency Int. Circuits Symp.*, May 2010.

[17] "2.4 GHz bluetooth low energy system-on-chip," [Online]. Available: http://www.ti.com/lit/ds/symlink/cc2540.pdf

[18] "Channel modeling for body area networks," IEEE P802.15-08-0780-12-0006 Nov. 2010.

[19] "Channel models for WBANs-NICT," IEEE P802.15-08-0416-04-0006 Nov. 2008.

[20] "Channel models for WBAN-holst centre/IMEC-NL," IEEE P802.15-08-0418-01-0006 Jul. 2008.

[21] "Narrowband channel characterization for body area networks," IEEE P802. 15-08-0421-00-0006 Jul. 2008.

[22] Y. Zhao *et al.*, "A simulation environment for subject-specific radio channel modeling in wireless body sensor networks," *Wearable Implantable Body Sensor Netw.*, pp. 23–28, Jun. 2009.

[23] C. Oliveira *et al.*, "Characterizing on-body wireless sensor networks," *New Technol., Mobil. Security*, pp. 1–6, Nov. 2008.

[24] J. Zhang *et al.*, "Stability of narrowband dynamic body area channel," *IEEE Antennas Wireless Propagat. Lett.*, pp. 53–56, 2009.

[25] D. Smith *et al.*, "Characterization of the dynamic narrowband on-body to off-body area channel," in *IEEE Int. Conf. Commun.*, Jun. 2009, pp. 1–6.

[26] J. K. Holmes, *Spread spectrum systems for GNSS and wireless communications*. Boston, MA: Artech, 2007.

[27] K. M. Silva *et al.*, "Network topologies for dual band (UWB—transmit and narrow band-receive) wireless body area network," in *Proc. 4th Int. Conf. Body Area Netw.*, Beijing, China, 2011.

Nathan E. Roberts received the B.S. degree in electrical engineering from the University of San Diego, San Diego, CA, in 2006 and the M.S. degree in electrical engineering from the University of Michigan, Ann Arbor, in 2011, where he is currently pursuing the Ph.D. degree.

From 2006 to 2009, he held a position with the Product Development Engineering division at Lattice Semiconductor, Hillsboro, OR. His research interests include the design of low-power wireless integrated circuits for energy-constrained systems.

Seunghyun Oh received the B.S. degree in electrical engineering from Seoul National University, Seoul, Korea, in 2007, and the M.S. degree in electrical engineering from the University of Michigan, Ann Arbor, in 2009.

His research interests include RF integrated circuits and communication in body area networks.

Mr. Oh is the recipient of the Korea Foundation for Advanced Studies Fellowship.

David D. Wentzloff (M'02) received the B.S.E. degree in electrical engineering from the University of Michigan, Ann Arbor, in 1999, and the S.M. and Ph.D. degrees from the Massachusetts Institute of Technology, Cambridge, in 2002 and 2007, respectively.

In the summer of 2004, he worked in the Portland Technology Development group at Intel in Hillsboro, OR. Since August, 2007 he has been with the University of Michigan, Ann Arbor, where he is currently an Assistant Professor of Electrical Engineering and Computer Science. He has served as a Guest Editor of the Elsevier *Journal of Signal Processing: Image Communication*.

Dr. Wentzloff is the recipient of the 2002 MIT Masterworks Award, 2004 Analog Devices Distinguished Scholar Award, 2009 DARPA Young Faculty Award, the 2009–2010 Eta Kappa Nu Professor of the Year Award, and the 2011 DAC/ISSCC Student Design Contest Award. He has served on the technical program committee for ICUWB 2008–2010 and ISLPED 2011–2012, and as a Guest Editor for the IEEE TRANSACTIONS ON MICROWAVE THEORY AND TECHNIQUES and the IEEE COMMUNICATIONS MAGAZINE. He is a member of Tau Beta Pi.